Research Article | Vol. 26, No. 10 | 14 May 2018 | OPTICS EXPRESS 12648
Optics EXPRESS

Gas-lens effect in kW-class thin-disk lasers

A. DIEBOLD,[1,3] F. SALTARELLI,[1,3,*] I. J. GRAUMANN,[1] C. J. SARACENO,[1,2] C. R. PHILLIPS,[1] AND U. KELLER[1]

[1]*Ultrafast Laser Physics, Institute for Quantum Electronics, ETH Zurich, Zurich, Switzerland*
[2]*Photonics and Ultrafast Laser Science, Ruhr-Universität Bochum, Bochum, Germany*
[3]*These authors contributed equally to this work.*
[*]*saltarelli@phys.ethz.ch*

Abstract: We unveil a gas-lens effect in kW-class thin-disk lasers, which accounts in our experiments for 33% of the overall disk thermal lensing. By operating the laser in vacuum, the gas lens vanishes. This leads to a lower overall thermal lensing and hence to a significantly extended power range of optimal beam quality. In our high-power continuous-wave (cw) thin-disk laser, we obtain single-transverse-mode operation, i.e. $M^2 < 1.1$, in a helium or vacuum environment over an output-power range from 300 W to 800 W, which is 70% broader than in an air environment. In order to predict the magnitude of the gas-lens effect in different thin-disk laser systems and gain a deeper understanding of the effect of the heated gas in front of the disk, we develop a new numerical model. It takes into account the heat transfer between the thin disk and the surrounding gas and calculates the lensing effect of the heated gas. Using this model, we accurately reproduce our experimental results and additionally predict, for the first time by means of a theoretical tool, the existence of the known gas-wedge effect due to gas convection. The gas-lens and gas-wedge effects are relevant to all high-power thin-disk systems, both oscillators and amplifiers, operating in cw as well as pulsed mode. Specifically, canceling the gas-lens effect becomes crucial for kW power scaling of thin-disk oscillators because of the larger mode area on the disk and the resulting higher sensitivity to the disk thermal lens.

OCIS codes: (140.0140) Lasers and laser optics; (140.3615) Lasers, ytterbium; (140.6810) Thermal effects; (350.6830) Thermal lensing.

References and links

1. U. Keller, "Recent developments in compact ultrafast lasers," Nature **424**(6950), 831–838 (2003).
2. K. Sugioka and Y. Cheng, "Ultrafast lasers - reliable tools for advanced materials processing," Light Sci. Appl. **3**(4), e149 (2014).
3. T. Südmeyer, S. V. Marchese, S. Hashimoto, C. R. E. Baer, G. Gingras, B. Witzel, and U. Keller, "Femtosecond laser oscillators for high-field science," Nat. Photonics **2**(10), 599–604 (2008).
4. M. N. Zervas and D. A. Codemard, "High Power Fiber Lasers: A Review," IEEE J. Sel. Top. Quantum Electron. **20**(5), 0904123 (2014).
5. P. Russbueldt, D. Hoffmann, M. Hofer, J. Lohring, J. Luttmann, A. Meissner, J. Weitenberg, M. Traub, T. Sartorius, D. Esser, R. Wester, P. Loosen, and R. Poprawe, "Innoslab Amplifiers," IEEE J. Sel. Top. Quantum Electron. **21**(1), 3100117 (2015).
6. A. Giesen, H. Hügel, A. Voss, K. Wittig, U. Brauch, and H. Opower, "Scalable Concept for Diode-Pumped High-Power Solid-State Lasers," Appl. Phys. B **58**(5), 365–372 (1994).
7. S.-S. Schad, T. Gottwald, V. Kuhn, M. Ackermann, D. Bauer, M. Scharun, and A. Killi, "Recent development of disk lasers at TRUMPF," Proc. SPIE **9726**, 972615 (2016).
8. V. Kuhn, T. Gottwald, C. Stolzenburg, S.-S. Schad, A. Killi, and T. Ryba, "Latest advances in high brightness disk lasers," Proc. SPIE **9342**, 93420Y (2015).
9. J.-P. Negel, A. Loescher, A. Voss, D. Bauer, D. Sutter, A. Killi, M. A. Ahmed, and T. Graf, "Ultrafast thin-disk multipass laser amplifier delivering 1.4 kW (4.7 mJ, 1030 nm) average power converted to 820 W at 515 nm and 234 W at 343 nm," Opt. Express **23**(16), 21064–21077 (2015).
10. T. Nubbemeyer, M. Kaumanns, M. Ueffing, M. Gorjan, A. Alismail, H. Fattahi, J. Brons, O. Pronin, H. G. Barros, Z. Major, T. Metzger, D. Sutter, and F. Krausz, "1 kW, 200 mJ picosecond thin-disk laser system," Opt. Lett. **42**(7), 1381–1384 (2017).
11. M. Schultze, S. Klingebiel, C. Wandt, C. Y. Teisset, R. Bessing, M. Haefner, S. Prinz, K. Michel, and T. Metzger, "500 W - 10 mJ - Picosecond Thin-Disk Regenerative Amplifier," Europhoton Conference 2016, SSL-5.4.

#327820 https://doi.org/10.1364/OE.26.012648
Journal © 2018 Received 9 Apr 2018; accepted 23 Apr 2018; published 2 May 2018

Optics EXPRESS

12. J. Aus der Au, G. J. Spühler, T. Südmeyer, R. Paschotta, R. Hövel, M. Moser, S. Erhard, M. Karszewski, A. Giesen, and U. Keller, "16.2-W average power from a diode-pumped femtosecond Yb:YAG thin disk laser," Opt. Lett. **25**(11), 859–861 (2000).
13. C. J. Saraceno, F. Emaury, O. H. Heckl, C. R. E. Baer, M. Hoffmann, C. Schriber, M. Golling, T. Südmeyer, and U. Keller, "275 W average output power from a femtosecond thin disk oscillator operated in a vacuum environment," Opt. Express **20**(21), 23535–23541 (2012).
14. J. Brons, V. Pervak, D. Bauer, D. Sutter, O. Pronin, and F. Krausz, "Powerful 100-fs-scale Kerr-lens mode-locked thin-disk oscillator," Opt. Lett. **41**(15), 3567–3570 (2016).
15. F. Emaury, A. Diebold, A. Klenner, C. J. Saraceno, S. Schilt, T. Südmeyer, and U. Keller, "Frequency comb offset dynamics of SESAM modelocked thin disk lasers," Opt. Express **23**(17), 21836–21856 (2015).
16. S. V. Marchese, C. R. E. Baer, A. G. Engqvist, S. Hashimoto, D. J. H. C. Maas, M. Golling, T. Südmeyer, and U. Keller, "Femtosecond thin disk laser oscillator with pulse energy beyond the 10-microjoule level," Opt. Express **16**(9), 6397–6407 (2008).
17. C. J. Saraceno, F. Emaury, C. Schriber, A. Diebold, M. Hoffmann, M. Golling, T. Südmeyer, and U. Keller, "Toward millijoule-level high-power ultrafast thin-disk oscillators," IEEE J. Sel. Top. Quantum Electron. **1**, 1100318 (2015).
18. V. Magni, "Multielement stable resonators containing a variable lens," J. Opt. Soc. Am. A **4**(10), 1962–1969 (1987).
19. S. Piehler, T. Dietrich, P. Wittmüss, O. Sawodny, M. A. Ahmed, and T. Graf, "Deformable mirrors for intra-cavity use in high-power thin-disk lasers," Opt. Express **25**(4), 4254–4267 (2017).
20. B. Weichelt, A. Voss, M. A. Ahmed, and T. Graf, "Enhanced performance of thin-disk lasers by pumping into the zero-phonon line," Opt. Lett. **37**(15), 3045–3047 (2012).
21. B. Weichelt, D. Blazquez-Sanchez, A. Austerschulte, A. Voss, T. Graf, and A. Killi, "Improving the brightness of a multi-kW thin disk laser with a single disk by an aspherical phase-front correction," Proc. SPIE **7721**, 77210M (2010).
22. T. Dietrich, S. Piehler, C. Röcker, M. Rumpel, M. Abdou Ahmed, and T. Graf, "Passive compensation of the misalignment instability caused by air convection in thin-disk lasers," Opt. Lett. **42**(17), 3263–3266 (2017).
23. J.-P. Negel, A. Voss, M. A. Ahmed, D. Bauer, D. Sutter, A. Killi, and T. Graf, "1.1 kW average output power from a thin-disk multipass amplifier for ultrashort laser pulses," Opt. Lett. **38**(24), 5442–5445 (2013).
24. G. Zhu, X. Zhu, M. Wang, Y. Feng, and C. Zhu, "Analytical model of thermal effect and optical path difference in end-pumped Yb:YAG thin disk laser," Appl. Opt. **53**(29), 6756–6764 (2014).
25. C. J. Saraceno, F. Emaury, C. Schriber, M. Hoffmann, M. Golling, T. Südmeyer, and U. Keller, "Ultrafast thin-disk laser with 80 μJ pulse energy and 242 W of average power," Opt. Lett. **39**(1), 9–12 (2014).
26. K. Schuhmann, K. Kirch, and A. Antognini, "Multi-pass oscillator layout for high-energy mode-locked thin-disk lasers," https://arxiv.org/abs/1603.00404 (2016).
27. D. Bauer, I. Zawischa, D. H. Sutter, A. Killi, and T. Dekorsy, "Mode-locked Yb:YAG thin-disk oscillator with 41 μJ pulse energy at 145 W average infrared power and high power frequency conversion," Opt. Express **20**(9), 9698–9704 (2012).
28. K. Schuhmann, K. Kirch, F. Nez, R. Pohl, and A. Antognini, "Thin-disk laser scaling limit due to thermal lens induced misalignment instability," Appl. Opt. **55**(32), 9022–9032 (2016).
29. C. R. E. Baer, O. H. Heckl, C. J. Saraceno, C. Schriber, C. Kränkel, T. Südmeyer, and U. Keller, "Frontiers in passively mode-locked high-power thin disk laser oscillators," Opt. Express **20**(7), 7054–7065 (2012).
30. S. Chenais, F. Balembois, F. Druon, G. Lucas-Leclin, and P. Georges, "Thermal lensing in diode-pumped ytterbium lasers - Part I: Theoretical analysis and wavefront measurements," IEEE J. Quantum Electron. **40**(9), 1217–1234 (2004).
31. J. Shang, X. Zhu, and G. Zhu, "Analytical approach to thermal lensing in end-pumped Yb:YAG thin-disk laser," Appl. Opt. **50**(32), 6103–6120 (2011).
32. J. Perchermeier and U. Wittrock, "Precise measurements of the thermo-optical aberrations of an Yb:YAG thin-disk laser," Opt. Lett. **38**(14), 2422–2424 (2013).
33. R. Penndorf, "Tables of the Refractive Index for Standard Air and the Rayleigh Scattering Coefficient for the Spectral Region between 0.2 and 20.0 μ and Their Application to Atmospheric Optics," J. Opt. Soc. Am. **47**(2), 176–182 (1957).
34. J. A. Stone and A. Stejskal, "Using helium as a standard of refractive index: correcting errors in a gas refractometer," Metrologia **41**(3), 189–197 (2004).
35. E. R. Peck and B. N. Khanna, "Dispersion of Nitrogen," J. Opt. Soc. Am. **56**(8), 1059–1063 (1966).

1. Introduction

Increasing the average output power from diode-pumped solid-state lasers is motivated by many industrial and scientific applications [1–3]. Reaching the desired kW-class performance requires gain materials with both excellent thermal properties and optimized heat-removal designs. In particular, Yb-doped materials have been at the forefront of most high-power continuous-wave (cw) laser developments in the last few decades. In addition to a small

Optics EXPRESS

quantum defect, they exhibit broad absorption spectra in the near-infrared, which are easily accessible by low-cost high-power diode pump lasers.

Three different design architectures have proved especially successful for state-of-the-art thermal management: fiber [4], slab [5], and thin-disk [6] geometries. In the scope of this paper, we focus on the thin-disk design, which, specifically, is well suited for applications requiring excellent spatial beam quality. Here, the gain medium is shaped as a disk with a thickness in the order of 100 µm and used in reflection with cavity mode sizes in the mm range. The large ratio of pump-spot size to disk thickness results in a quasi-1D heat flow through the backside of the disk and strongly reduces thermal-lensing effects. Thanks to this feature, power scaling is possible by simply increasing simultaneously the pump power and the pump-spot size on the disk, while keeping the pump intensity constant. This power scalability led to the demonstration of more than 10 kW of output power in cw operation from a multimode ($M^2 > 10$) thin-disk laser (TDL) with a single disk [7], or up to 4 kW with a lower M^2 of 1.4 [8]. However, in this latter result an $M^2 < 2.0$ was only achieved at output powers between 3 kW and 4 kW, thus in a comparatively narrow range of 1 kW.

The thin-disk concept allows for exceptional results also in high-power ultrafast operation. In a multi-pass thin-disk amplifier setup, 1.4 kW at 300 kHz repetition rate with 8-ps pulses were demonstrated at an $M^2 > 1.4$ [9]. Also, thin-disk regenerative amplifiers made large progress in recent years with up to 1 kW of average output power at 5 kHz [10] or 500 W at 50 kHz [11], both at 1 ps of pulse duration.

For even higher pulse repetition rates in the MHz range, modelocked ultrafast TDLs [12] are particularly attractive as they generate few hundreds of Watts of average power directly from a compact oscillator at sub-ps pulse durations [13, 14]. Furthermore, they offer excellent single-transverse-mode beam quality with an $M^2 < 1.1$ and low noise properties [15]. Often, these systems are operated in helium (He) or vacuum environments to avoid excessive nonlinearities [14, 16, 17]. For a stable intracavity pulse-formation process, higher-order modes must be prevented [17]. Thus, modelocked TDLs are also very demanding when it comes to the thermal-lensing behavior of the disk. In particular, for high output powers approaching the kW level, a large spot size (i.e., with a diameter close to 10 mm) is required on the disk. In TDLs, the width of the stability zone with respect to disk thermal lensing scales inversely with the square of the pump-spot size, for a fixed number of intracavity passes over the gain material [18]. Thus, increased spot sizes result in an increased sensitivity to the disk thermal lensing, which makes it more challenging to achieve single-mode operation over a wide power range. The disk thermal lensing can be compensated for by using deformable mirrors in TDLs in order to dynamically adjust the cavity during operation [19]. This, however, comes at the expense of additional complexity in the laser setup. Additionally, the thermal load on the disk and consequently the thermal lensing can be mitigated by pumping into the zero-phonon line at 969 nm instead of 940 nm [20].

Through many years of industrial-scale research, thin disks, specifically based on the gain material Yb:YAG, have been optimized in terms of optical and thermal behavior [8]. Yet, in addition to thermo-optic effects intrinsic to the disk, the heated gas atmosphere close to the disk can have a significant impact on the laser performance. One effect, which recently received experimental attention, is the so-called gas wedge. It is a vertical deflection of the beam caused by an asymmetric vertical temperature profile of the heated gas in front of the disk. Measures to compensate for this gas-wedge effect include adjustments of the cavity end mirrors, He-flooding the laser [21], introduction of an angularly dispersive element [22], or the use of retroreflectors in multi-pass thin-disk amplifiers [23]. However, neither a systematic understanding of the gas wedge nor a measurement of the full influence of the gas environment on the thin-disk thermal-lensing behavior has been demonstrated to date.

In this paper, we investigate the disk thermal-lensing effects of high-power TDL systems in different gas environments. In our cw TDL setup, we achieve single-mode operation (i.e. $M^2 < 1.1$) over an approximately 70% broader output-power range of about 500 W in vacuum

Optics EXPRESS

(i.e. 1 mbar) versus about 300 W in air (Fig. 1). At a first glance, this result appears counter-intuitive as one might expect more severe thermal effects in the absence of air (i.e. in vacuum), and thus a narrower output power range of good mode quality. To investigate the observed behavior in detail, we carry out a thermal-lensing measurement for our state-of-the-art disk in different gas environments. We find a reduction of the overall disk thermal lens by ~33% when operating in vacuum or 1 bar of He as compared to 1 bar of air or 1 bar of nitrogen (N_2), with the disk temperature being independent of the gas environment. In a newly developed numerical simulation, we modeled our experimental results with a gas lens induced by the heated gas in front of the thin disk, which adds to the disk-material thermal effects analyzed in Ref [24]. This gas lens is non-existent for vacuum environments and roughly a factor of five smaller for He as compared to air and N_2. Our model also predicts the above-mentioned gas-wedge effects and forecasts a reduction of this effect by an order of magnitude when going from air to He.

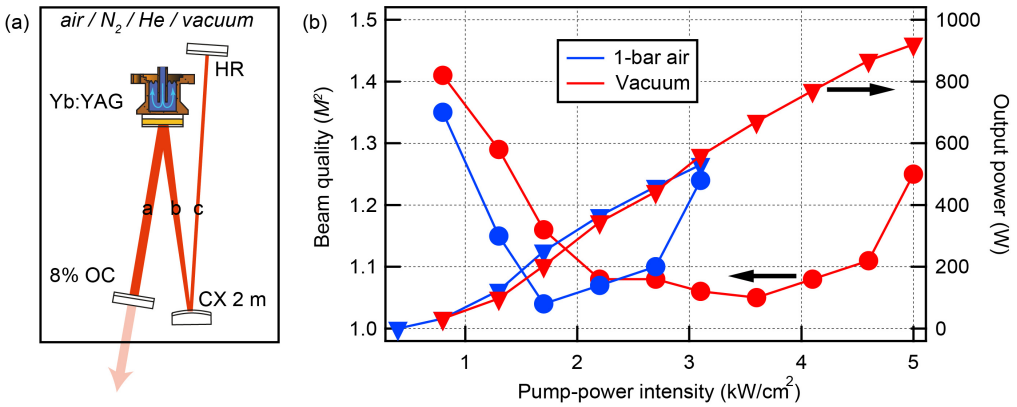

Fig. 1. (a) Schematic of the single-mode cw thin disk laser (TDL) cavity setup, including an output coupler (OC), a 2-m convex (CX) mirror, and the highly-reflective (HR) end mirror. The three cavity arms are labeled as *a*, *b*, and *c*, respectively. (b) Output-power slope for high-power single-mode operation. The power range of good beam quality (i.e. $M^2 < 1.1$) is ~70% broader in vacuum as compared to 1-bar air.

Our findings therefore provide crucial knowledge for the design of the next generation of TDL systems. In particular, we suggest operating the cavity in a low-pressure environment or flooding it with helium in order to remove the gas-lens and gas-wedge effects and significantly increase the operation range of high-power TDLs. Thin-disk cavities with high sensitivity to disk thermal lensing will particularly benefit from our investigation. Such systems include those with output powers in the kW range and consequently large disk spot sizes, as well as high-energy thin-disk lasers with multiple passes over the gain crystal [25–27]. For ultrafast high-power TDLs, the suggested approach is particularly attractive as replacing air with helium or vacuum additionally heavily reduces intracavity nonlinearities [17].

The paper is structured as follows. In section 2, we present our high-power single-mode TDL cw results in different gas environments. Section 3 details our thermal-lensing measurements, including the discovery of a gas lens in front of the disk. Our findings indicate a significant difference of operation in 1-bar air and 1-bar N_2 as compared to vacuum and 1-bar He and thus explain our laser experiments. Section 4 theoretically models our experiments, discussing both the gas-lens and the gas-wedge effect. We conclude in section 5.

2. High-power single-transverse-mode TDL operation

In our experimental high-power single-mode TDL setup, we used a 100-µm-thick, 10-at.%-doped, 3.80-m-curved Yb:YAG disk with a diameter of 20 mm, bonded onto a

Optics EXPRESS

diamond heat sink. The disk was inserted into a 44-pass thin-disk laser head and pumped with a free-space-coupled diode, delivering up to 3.7 kW at at center wavelength of 940 nm. The pumping scheme resulted in an 8-mm-diameter octagonal-shaped pump spot. The above-mentioned parts were provided by Trumpf. We placed the entire setup inside a vacuum chamber, similar to the one used in [13], which allowed for operation in either air, vacuum (~1 mbar), He, or N_2 environment.

We designed a single-mode cavity with a single reflection on the disk [Fig. 1(a)]. It consisted of three arms, with lengths a = 1000 mm, b = 1100 mm, and c = 2308 mm. This cavity setup was convenient due to its independent adaptability of both the laser-mode radius on the disk via arm c, and the center of the cavity stability zone [18, 28, 29] with respect to the disk thermal lens via arm b. For an experimentally optimized beam quality, we chose a laser-mode radius on the disk of 2.87 mm in the center of the stability zone, leading to an overlap with the pump spot of ~72%. The cavity was operated with an output-coupling (OC) mirror transmission of 8% and its alignment was optimized during operation via piezo-controlled cavity end mirrors. We increased the OC rate to 8% from 4% used for the multimode operation in order to reduce the intracavity power. In fact, compared to multimode operation, in the single mode cavity we have a smaller beam on the intracavity mirrors and so higher intensities.

In this setup, we measured in cw operation simultaneously the output power and the beam quality (M^2) of the output laser mode. We always refer to the average M^2 value, i.e. $M^2 = sqrt(M^2_x * M^2_y)$. Using different gas environments and keeping all other cavity parameters constant, we pumped the disk up to 2.5 kW of pump power, corresponding to a pump intensity of 5 kW/cm^2. As we show in Fig. 1(b), we achieved good beam quality ($M^2 < 1.1$) for operation in vacuum from ~300 W to ~800 W of output power, i.e. over a power range of ~500 W. In 1-bar air, this range narrowed down to ~200 W to ~500 W, i.e. a power range of ~300 W. In 1-bar He, we achieved similar results as in vacuum, and in 1-bar N_2 similar results as in 1-bar air. For the sake of clarity, the data points for 1-bar N_2 and 1-bar He are omitted from Fig. 1. We could shift the center of the power range of good beam quality to different output power levels by adapting arm b. Yet, the overall span of the ranges stayed unchanged for each gas environment.

Our observations suggest a reduced disk thermal lensing in vacuum or 1-bar He as compared to 1-bar air or 1-bar N_2. This led us to investigate the origins of thermal lensing in our system in more detail, as a broad power range of good beam quality is crucial, in particular for modelocked operation.

3. Thermal-lensing measurements

3.1 Experimental setup

We simultaneously employed two independent diagnostics to measure the thermal-lensing behavior of our thin disk.

1. Interferometer: We used the interferometer Trioptics µPhase PLANO S DOWN with a frequency-stabilized HeNe Laser, routed into our vacuum-chamber with a 4-f 1:1 imaging setup.

   For each gas environment, we treated the radius of curvature of the cold disk as a reference point and we measured deviations from that. In this way, we can measure small changes, independent of the absolute calibration of the reference surface. Given the measured phase profile, to obtain the lensing effect we first set an analysis mask for the interferometer laser beam on the disk, filling the whole 8 mm pump spot size, and then perform a fit to obtain a lens value in diopters. Thus, we calculated the total disk thermal lens as $\Delta F_{total} = 2/R(I) - 2/R(I = 0)$, where R is the disk's radius of curvature and I is the pump intensity on the disk. From the fits, the

Optics EXPRESS

uncertainty that we get on ΔF_{total} is <0.3 x 10^{-3} diopters. Thus, we do not expect this to be the limiting factor in the precision of our measurements.

2. Laser focus: As a second method, we directly measured on a beam profiler the focusing effect experienced by a probe beam upon reflection from the disk.

   For this method, we set up a single-frequency diode laser (Toptica CTL 1050) and collimated its single-mode output beam with 6.80-mm $1/e^2$ diameter on the disk. We tuned its wavelength to 1060 nm to minimize the gain effect of the disk on the probe beam. We measured the $1/e^2$ beam diameter w_{cam} with a DataRay WinCamD-LCM camera at a distance d_{cam} = 2.40 m from the disk. Given the probe beam size on the disk and the distance d_{cam}, through ABCD matrix calculations it is possible to relate the beam size at the camera position with the disk radius of curvature and, ultimately, with its thermal lensing ΔF_{total}. We chose the position d_{cam} in order to have a good compromise between the sensitivity to thermal lensing ($\partial w_{cam}/\partial \Delta F_{total}$) and the beam diameter w_{cam} with respect to the camera aperture. With the chosen d_{cam}, at ΔF_{total} = 0, we have w_{cam} = 1.8 mm and a sensitivity $\partial w_{cam}/\partial \Delta F_{total}$ = 8 mm/m^{-1}. With a pixel size of (5.5x5.5) μm^2, this sensitivity translates to a minimum measurable variation on ΔF_{total} of 0.7 x 10^{-3} diopters. This value is comparatively small with respect to the measured thermal lensing. Additionally, we took sample profiles every 0.5° in the camera image and for each one we calculated w_{cam}. We obtained the final value of w_{cam} averaging them. Thus, also in this case, we do not expect the precision on ΔF_{total} to be limited by the measuring technique.

In order to assess the repeatability of our ΔF_{total} measurements, we repeated the same measures in different runs few hours apart. The recorded fluctuations in ΔF_{total} were in the percent-level.

In addition to the above measurements, the disk temperature was tracked with a calibrated thermal camera FLIR SC640, looking into the vacuum chamber through a Germanium window.

3.2 Measurement results and implication for kW-class TDL cavity

In all presented configurations, the disk defocused, i.e. the disk focal power decreased, with increasing pump power. However, the rate of change with respect to pump power depended on the exact operating conditions.

In fluorescence operation, the disk diopter change, relative to the cold disk, was linear versus pump power, within the range studied. Furthermore, thermal-lensing effects were of the same magnitude for operation in 1-bar air or 1-bar N_2, and 33% less pronounced in vacuum or 1-bar He. The disk temperature increased linearly with pump power and was independent of the gas environment. Figure 2(a) shows our fluorescence measurements. For the sake of clarity, we excluded the data points for 1-bar N_2. The experimental results from both measurement methods (interferometer and laser focus) stood in good agreement with each other within a ~10% error margin.

Optics EXPRESS

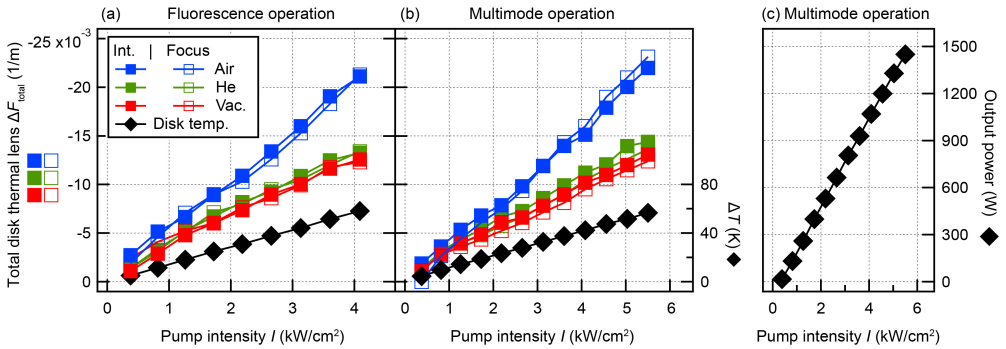

Fig. 2. (a) Disk thermal-lensing measurements in fluorescence mode, total disk thermal lens ΔF_{total}, disk peak temperature change ΔT. Both methods, interferometer (Int.) and laser focus (Focus), stand in good agreement with each other. Measurements in vacuum yielded similar results as 1-bar He, and measurements in 1-bar N_2 (not shown here) yielded similar results as 1-bar air. The disk-temperature increase is independent of the gas environment. (b) Disk thermal-lensing measurements in multimode (MM) operation, reaching 1.4 kW of output power [see Fig. 2(c)]. Due to the low sensitivity of the highly multimode test cavity to the cavity element curvatures, the output power was independent of the gas environment within the uncertainty of the used power meter (~5%). Note also that a slightly wider range of pump intensities (up to 5.5 kW/cm^2) is used for the multimode data.

Additionally, we measured the disk curvature in multimode (MM) laser operation. In this case the laser had an M^2 ~60, using a V-shaped cavity with a flat highly reflective (HR) mirror and a flat 4% OC mirror. We achieved MM output powers up to 1400 W. Thanks to the low sensitivity of the highly multimode test cavity to the cavity element curvatures, the output power was almost independent of the disk thermal lensing and of the different gas environments. We therefore only show one averaged curve in Fig. 2(c) for the output power. Again, thermal-lensing effects in vacuum or 1-bar He were ~33% weaker as compared to 1-bar air or 1-bar N_2. The absolute disk thermal lensing and temperature increase were reduced by ~25% in MM operation as compared to fluorescence operation, for the whole range of pump powers used in these experiments. This trend is expected from general heat fraction theory [30].

From both the fluorescence and MM measurements we found that the disk thermal lensing relates linearly to the disk peak temperature. We used the experimental data presented in Fig. 2 in order to calculate the ratio between the ΔF_{total} and the disk temperature increase ΔT through a linear fit with the intercept fixed to 0. We report this scale factor in the first two columns of Table 1 for fluorescence operation and multimode operation, respectively. The scale factor mostly depends on the gas environment, but is almost independent of the laser operating conditions (e.g., fluorescence, multimode, single mode). We therefore infer that the disk temperature is a quantitatively accurate metric for disk thermal lensing, with the scale factor found via the measurements presented in this section. From the mentioned linear fits, we could calculate an uncertainty on the presented fitting parameters of ~3%. Then, we use the vacuum measurements to isolate the gas contribution from the disk-material contribution obtaining the results presented in column 3 of Table 1. The mentioned uncertainties on the fit parameter allows us to provide an uncertainty on the gas-lens contribution $\Delta F_{\text{gas,exp}}/\Delta T$.

Optics EXPRESS

Table 1. Slope of disk thermal lensing for different gas environments. Total diopter change (ΔF_{total} , see also Fig. 2) in both fluorescence and multimode operation, diopter change due to the gas-lens effect ($\Delta F_{gas,exp} = \Delta F_{total} - \Delta F_{vacuum}$) inferred from the fluorescence measurement, and simulated diopter change due to the gas-lens effect ($\Delta F_{gas,sim}$, see section 4), all per disk peak temperature increase (ΔT). The fit uncertainty of ($\Delta F_{total} / \Delta T$) is ~3%. The resulting uncertainty of $\Delta F_{gas,exp} / \Delta T$ is presented in the table.

Gas environment	Fluorescence $\Delta F_{total} / \Delta T$ [10^{-6} 1/m/K]	Multimode $\Delta F_{total} / \Delta T$ [10^{-6} 1/m/K]	$\Delta F_{gas,\,exp} / \Delta T$ [10^{-6} 1/m/K]	$\Delta F_{gas,sim} / \Delta T$ [10^{-6} 1/m/K]
Vacuum	228	237	-	-
1-bar He	244	263	16 ± 6	26
1-bar air	364	374	136 ± 6	128
1-bar N_2	378	369	150 ± 12	143

The air temperature in the laboratory was 24 °C, and the humidity ~30%. Our measurements in N_2 show a difference for the $\Delta F_{gas,exp}/\Delta T$ with respect to air within 10% for both fluorescence (Table 1) and multimode operation. Thus, humidity did not strongly influence the gas-lens effect.

Thermal-lensing measurements in our kW-class single-mode setup described in section 2 (Fig. 1) were not possible due to space constraints in our cavity setup. Yet, the disk thermal lensing is directly proportional to the disk temperature. Thus, we measured the disk temperature increase during lasing and then inferred its thermal lens (from the results presented in Table 1). In Fig. 3(b), we present the measured M^2 as a function of the disk thermal lens. We overlap it with the corresponding calculated laser-beam radius at the disk, i.e. the stability zone. As in Fig. 1, we show two cases, 1-bar air and vacuum. The same set of measurements are used for both Fig. 1(b) and 3(b).

For each gas medium, a good M^2 occurred over the same range of thermal-lensing values. However, for vacuum and 1-bar He environments, where gas lensing is much weaker, this corresponds to a wider range of pump powers, and hence a wider range of output powers. The beam quality degraded as soon as the laser-beam radius at the disk, and therefore the overlap between laser beam and pump beam, deviated from the optimum value at the center of the stability zone.

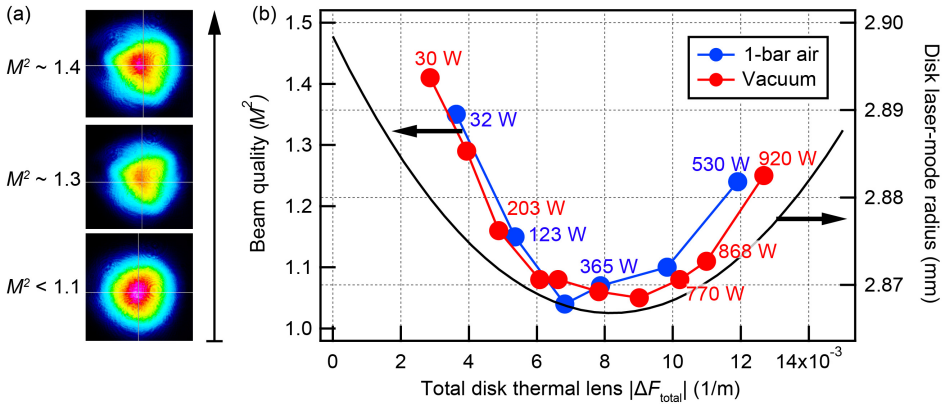

Fig. 3. (a) Sample output beam profile for different values of M^2. (b) Calculated stability zone of the single-mode cavity (black solid line) in comparison to the measured mode quality (M^2) versus the total disk diopter change (ΔF_{total}) for both operation in 1-bar air and vacuum. The overlaid numbers indicate the corresponding output power, see also Fig. 1(b). In this particular cavity setup, an ideal overlap of pump spot and laser spot, leading to an $M^2 < 1.1$, is achieved for disk thermal lensing between $-5*10^{-3}$ 1/m and $-11*10^{-3}$ 1/m.

Optics EXPRESS

It should be noted that in TDLs the width of the stability zone scales inversely with the square of the pump-spot size, for a fixed number of intracavity passes over the gain material [18]. For state-of-the-art kW-level TDL operation large spot diameters (e.g. 8.0 mm as presented here) are required in order to reach sufficient pump powers, which results in narrower stability zones. Thus, minimizing the disk thermal effects as much as possible becomes critical. The stability zone also becomes narrower or splits up when the number of laser passes over the gain material is increased. This concept is frequently employed in high-energy thin-disk lasers in the form of multi-cavity [25, 26] or relay-imaging multi-pass designs [27]. Thus, already at comparatively small pump-spot sizes, these lasers can exhibit a strong sensitivity to the disk thermal lensing. This means that the correct choice of the gas environment can become crucial to reach good beam quality over a broad range of output powers.

4. Simulation of the gas-lens and gas-wedge effects

We performed simulations to understand, model, and predict the observed thermal-lensing effects in different gas environments.

The disk heats up upon the absorption of pump light. On the one hand, this leads to well-studied disk-material defocusing thermal-lensing effects [31, 32], which are mostly due to the disk bending and changes in the disk's thermo-optic coefficient dn/dT, where n is the refractive index and T the temperature. The deposited heat is transported through the disk's backside and the diamond heat-sink into the cooling water. Consequently, we experimentally found our disk temperature to be virtually independent of the gas environment [Fig. 1(a)].

Nonetheless, a small fraction of heat, accounting for about 0.1% of the total heat dissipated by the disk, is transferred to the gas in front of the disk. The resulting temperature distribution in the gas exhibits a strong radial dependency. Due to the gas thermo-optic coefficient, this results in a gas lens, which contributes to the net disk thermal lensing. Additionally, the heated gas rises in front of the disk due to convection effects, ultimately causing a gas wedge [21–23].

In order to quantify both the gas-lens and gas-wedge effects, we carried out a three steps simulation for all different studied gas environments. As input, we used a disk temperature profile based on our thermal-camera measurements.

In a first step, we simulated the temperature rise and convection of the air surrounding the disk using the non-isothermal flow and conjugate heat transfer modules of the finite-element method software COMSOL Multiphysics 5.2a. The model includes the thin YAG disk and a 20-mm-long cylinder of gas placed in front of it [Fig. 4(a)]. The backside of the disk is set to the cooling water temperature of 24 °C and the front side of the disk has a super-Gaussian temperature distribution. Based on a fit of the thermal-camera images, the disk temperature distribution was modeled with a super-Gaussian radial distribution of order four with a FWHM of 8 mm (a Gaussian distribution would be of order two). The peak value of the super-Gaussian was set to the measured peak value of the disk temperature profile. This temperature profile constitutes a heat source for the gas in front of the disk. The heat transfer and gas flow equations (laminar flow), including gravity, were then solved, resulting in the full three-dimensional temperature distribution of the gas. We used open boundary conditions at the surfaces of the gas cylinder. The gas flow was simulated under the assumption of weak compressibility. The calculated maximum Reynolds number is < 4 for a peak disk temperature of 100 °C, which confirms that laminar flow is dominant.

In a second step, we used the temperature distribution and combined it with the gas thermo-optic coefficient [33–35] to calculate the $n(x,y,z)-1$ distribution in front of the disk, see Fig. 5 for 1-bar air and 1-bar He. Using the three-dimensional Helmholtz equation in the paraxial approximation, we subsequently studied the evolution of an incoming Gaussian laser beam while impinging orthogonally on the disk and propagating through the gas. Our numerical calculation employed the split-step Fourier method.

Optics EXPRESS

By fitting the phase profile of the output beam with a second-order polynomial, we obtained in a last step the curvature of the output beam in both axes as well as the phase-front tilt. From this, we inferred both the defocusing gas-lens (i.e. $\Delta F_{\text{gas lens, sim}}$) and the gas-wedge effects.

Thus, for a given pump-spot configuration, the full simulation takes as input the measured peak temperature on the disk as well as the gas type and pressure, and outputs the gas-induced lens and wedge.

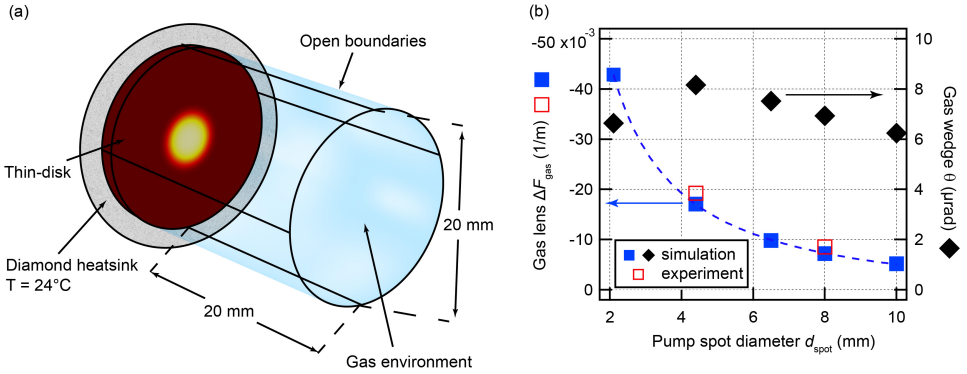

Fig. 4. (a) Schematic of the model showing, left to right, the diamond heatsink, the disk with the super-Gaussian temperature profile on it, and the gas in front of it. (b) Simulated and measured gas-lens and vertical-gas-wedge effect for a disk's peak temperature increase ΔT = 57 °C. We fitted the gas-lens-simulation data with the function $\Delta F_{\text{gas,sim}} = \alpha\,(d_{\text{spot}})^{\beta}$ finding β = −1.4. The gas-lens effect increases for smaller pump-spot diameter while the gas wedge (black squares) only slightly depends on it.

In all configurations, our model predicts a linear dependence of the gas-lens effect with respect to the disk temperature. We find a significant and similar gas lens in both 1-bar air and 1-bar N_2. The magnitude of the gas lens in air or N_2 is ~50% of our measured disk-material thermal-lensing effects, which we inferred from our experiments in vacuum. Thanks to the almost one order of magnitude lower (*n-1*) and *dn/dT* for helium (see Table 2), its gas-lens effect is roughly five times weaker as compared to air and therefore negligible in comparison to the disk-material thermal-lensing effects. We demonstrate a close agreement between simulation and experiment for the gas-lens effect in Table 1.

Table 2. Thermal and optical properties of vacuum, helium, nitrogen, and air, at 25°C and 1030 nm [33–35].

Gas	Index of refraction $(n\text{-}1)*10^4$	Thermo-optic coefficent $dn/dT*10^7$ [1/K]	Specific heat [J/(g*K)]	Thermal conductivity [W/(m*K)]
Vacuum	-	-	-	-
1-bar He	0.32	−1.06	5.19	0.15
1-bar air	2.65	−8.88	1.01	0.03
1-bar N_2	2.71	−9.15	1.04	0.03

Additionally, our model predicts the gas-wedge effect, which occurs due to gas convection [21–23]. From our simulations, we infer for 1-bar air and 1-bar N_2 an angular beam deviation θ linear to the disk temperature increase ΔT. This deviation is ~0.14 µrad/K in the vertical direction, and negligible in the horizontal direction (~0.005 µrad/K). For 1-bar He, the gas wedge in the vertical direction is roughly one order of magnitude smaller (~0.014 µrad/K), and for vacuum non-existent.

Experimental indications of such gas-wedge effects were observed before, but never quantified [21–23]. The influence of the gas wedge on the cavity is strongly dependent on the cavity design, particularly on the linear beam displacement Δy at the disk caused by an

Optics EXPRESS

angular beam deviation θ at the disk, i.e. $\Delta y = k * \theta$, where k is a sensitivity parameter. For the single-mode cavity presented in section 2, we calculate $k = -57$ mm/mrad. The sensitivity parameter translates into a gas-wedge-induced Δy of less than 0.5 mm at the maximum power in single-mode operation (i.e. for ΔT~60K). This is small compared to the 8.0 mm of pump-spot diameter on the disk. In fact, we could not experimentally measure the gas-wedge effect. However, in different cavity designs or with different disk materials, the gas wedge can play a more significant role. For instance, from the beam displacement presented in Fig. 4 of Ref [17]. and the corresponding cavity design, we can infer a gas-wedge effect of ~35 µrad in the vertical direction at ~2.5 kW/cm^2 of pump intensity. In this case, flooding the cavity with helium would be highly beneficial.

With our model, we performed a scan of the pump spot diameter on the disk finding that decreasing the spot size results in an increased gas-lens effect. In Fig. 4(b) we show the result of this scan for a disk's peak-temperature increase $\Delta T = 57$ °C. We fitted the simulations with the function $\Delta F_{gas,sim} = \alpha\ (d_{spot})^{\beta}$ finding $\beta = -1.4$. In order to confirm this trend we measured the gas-lens effect in a different laser with 4.4 mm pump-spot diameter finding a very good agreement with the scaling, as showed in the Fig. 4(b). Regarding the gas-wedge effect, we found out from the simulations that it only marginally depends on the pump spot diameter on the disk. The provided scaling function for the gas-lens effect can be used in order to estimate the magnitude of this effect in a thin-disk laser with a different pump spot size and thus assess what would be the beneficial effect of going to vacuum or helium flooding the chamber.

Finally, we investigated the sensitivity of our model to the shape of the temperature profile on the disk. A super-Gaussian of order 8 (i.e. a more flat-top profile) lead to an increase of the predicted gas-lens effect by ~10%.

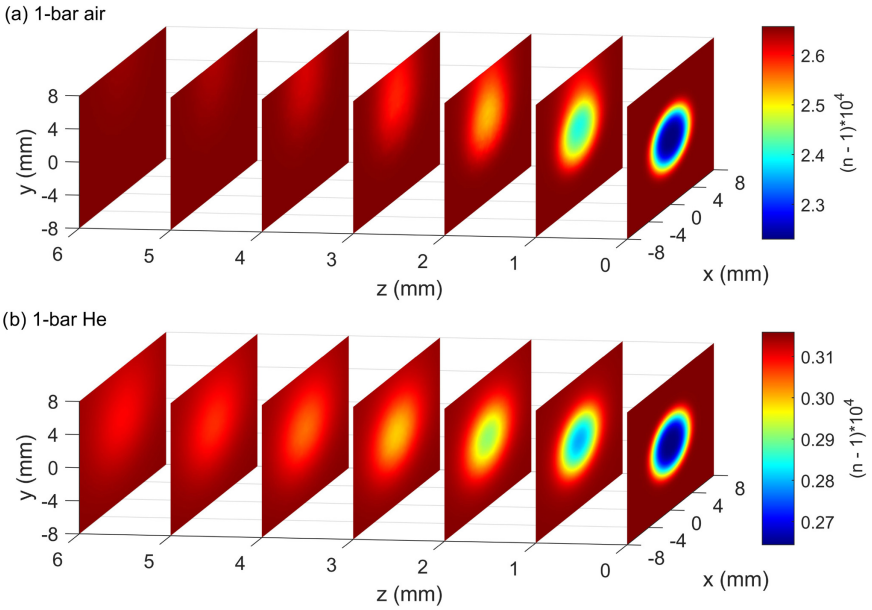

Fig. 5. Simulation of the gas refractive index ($n(x,y,z)-1$) profiles for (a) 1-bar air and (b) 1-bar He. The disk is situated at z = 0 mm with a peak temperature of 81 °C ($\Delta T = 57$ °C). Both the gas-lens and gas-wedge effects are clearly visible. Due to the higher thermal conductivity of He, see Table 2, the heat from the disk extends further into the gas. Nonetheless, thanks to the order of magnitude lower n-1, the thermo-optic effects for He are significantly less pronounced as compared to air, as in our experimental data summarized in Table 1.

Optics EXPRESS

5. Conclusion

We presented a detailed investigation of the disk thermal-lensing effects in high-power thin-disk lasers in different gas environments. We measured, for the first time, a reduction of the overall disk thermal lens by ~33% when operating our state-of-the-art disk in vacuum or 1 bar of He as compared to 1 bar of air or 1 bar of N_2. With this knowledge, we achieved in our high-power cw TDL setup single-mode operation, i.e. $M^2 < 1.1$, over a ~70% broader output power range of ~500 W in He or vacuum atmosphere versus a range of ~300 W in air. We anticipate that combining an air-purged environment with pumping at a wavelength of 969 nm, will further increase the power range of optimal beam quality.

Our simulations accurately modeled our experimental results with a gas lens induced by the heated gas in front of the thin disk, which adds on top of disk-material thermal effects. The gas lens is roughly five times weaker for He as compared to air and N_2, and non-existent for vacuum environments. In addition to the gas lens, our model predicts a gas wedge due to the inhomogeneous vertical temperature profile of the heated gas in front of the disk.

Our findings therefore provide crucial knowledge for the design of advanced thin-disk laser systems with output powers in the kW range and consequently large disk spot sizes, this includes high-energy thin-disk lasers with multiple intracavity passes over the gain crystal. Additionally, using vacuum or helium atmospheres cancels the gas wedge and heavily reduces intracavity nonlinearities, which is particularly attractive for ultrafast applications.

Funding

Swiss National Science Foundation (SNSF) (200020_172644); Sofja Kovalevskaja Award of the Alexander von Humboldt Foundation; Cluster of Excellence RESOLV (EXC 1069).

Acknowledgments

We would like to thank Trumpf Laser GmbH for providing the thin-disk equipment.